Numerical Modeling of Highly Swirling Flows in a Through-Flow Cylindrical Hydrocyclone

Jordan Ko, Said Zahrai, and Olivier Macchion
Dept. of Mechanics, Royal Institute of Technology, Stockholm, Sweden

Hannes Vomhoff
STFI-Packforsk, Stockholm, Sweden

DOI 10.1002/aic.10955
Published online August 11, 2006 in Wiley InterScience (www.interscience.wiley.com).

This article aims to identify the most appropriate numerical methodology for simulating hydrocyclone flows with high swirl numbers. The numerical results are validated against the tangential velocity measurements from a cylindrical hydrocyclone with a swirl number of 8.1, which is twice the typical swirl magnitude of industrial hydrocyclones. The linear and quadratic formulations of the Reynolds stress transport (RST) model are used to simulate the anisotropic swirling turbulent flow three-dimensionally in the commercial software package Fluent™. The tangential velocity profiles predicted by the quadratic RST model are in good agreement with experimental data. They also show Rankine vortex patterns over the entire flow domain. In contrast, the linear RST model fails to predict this important swirl flow feature. In addition, both models predicted a complex axial flow reversal pattern not previously reported in hydrocyclones. This study clearly shows that the quadratic RST model is preferable for future hydrocyclone simulations, especially when the swirl number is large. All necessary physical and numerical parameters used to obtain converged results are given in this article. © 2006 American Institute of Chemical Engineers *AIChE J,* 52: 3334–3344, 2006

Keywords: hydrocyclone separator, swirling flow, Reynolds stress transport models, turbulence

Introduction

In paper manufacturing, a pulp suspension is laid out on a continuously moving wire mesh and paper is obtained when most of the water is removed from the suspension. Paper properties can vary significantly depending on the morphology of the wood fibers that form the pulp suspension. The morphology of the fibers can be highly seasonally dependent. Faster spring growth results in thinner fiber walls, whereas slower summer growth leads to thicker fiber walls. Because of their different physical and optical characteristics, paper properties can be improved by first fractionating the fibers and then layering the appropriate fibers in a manner that optimizes paper strength, printability, and other desired qualities.[1]

Different devices can be used to fractionate fibers according to their physical characteristics. First introduced to remove low- or high-density contaminants from pulp suspension, hydrocyclones have long been used in the pulp and paper industry. In addition to contaminant removal, it is also possible to fractionate fibers according to their morphological differences with a hydrocyclone. Kure et al.[2] and Paavilainen[3] experimentally showed that hydrocyclones fractionate fibers according to their fiber wall thickness. The fractionation capability of a hydrocyclone relies on its large swirl flow. The feed flow, containing both thin-walled earlywood fibers and thick-walled latewood fibers, is injected tangentially to create the swirl. This

Correspondence concerning this article should be addressed to J. Ko at Ko.jordan@gmail.com.

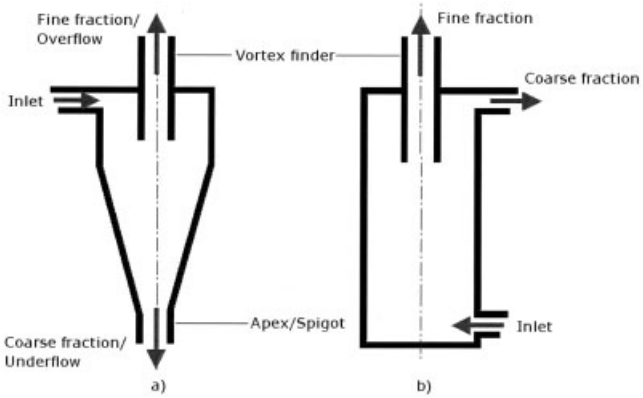

Figure 1. Outlines of a reverse-flow conical hydrocyclone and a through-flow cylindrical hydrocyclone.

swirling flow imparts a centrifugal acceleration to the fibers in the suspension. Because of the differences in the centrifugal forces caused by its larger relative densities and/or the differences in the drag forces caused by its smaller specific surfaces, latewood fibers are prone to sediment toward the hydrocyclone wall, whereas the earlywood fibers are likely to remain close to the hydrocyclone axis. Consequently, a coarse fraction composed mainly of latewood fibers collects near the wall and is extracted. In contrast, a fine fraction composed mainly of earlywood fibers exits by a separate opening. Although the term "hydrocyclone" denotes both the device and the flow medium, the term will be used herein to refer to the device that is the subject of study.

The outlines of a conical and a cylindrical hydrocyclone are shown in Figure 1. Tangential inlets are positioned at one end of the hydrocyclone to create the swirling component in the flow. An outlet termed the *vortex finder*, by which the fine fraction exits, is positioned along the hydrocyclone's geometric axis. In the conical hydrocyclone the coarse fraction exits by the axial apex at the end of the conical contraction and in the cylindrical hydrocyclone the coarse fraction exits by another tangential pipe. Typically, axial flow reversal takes place in the contraction region of the conical hydrocyclone. The hydrocyclone flow direction can be classified as reverse-flow or through-flow. In a reverse-flow hydrocyclone, part of the flow has to turn 180° to exit; in contrast, no change in the flow direction is caused by the orientations of the exits in through-flow hydrocyclone.

The tangential velocity profiles in hydrocyclones have similarities to a combination of free and forced vortices and this combined pattern, called a *Rankine vortex*, is a salient feature in hydrocyclone flows. A forced vortex is represented by a linearly increasing velocity with increasing radius and a free vortex is represented by an inversely decreasing velocity with increasing radius. The reference to free vortex here does not imply that the radial and axial velocity components are zero, as required in the potential flow theory. Another important hydrocyclone flow feature is the *precessing vortex core* (PVC), which is a continuous helical column of air that gathers in the low-pressure center in the rotational plane and it precesses about the geometric center at a high frequency.

The simulation of swirl flow in hydrocyclones is difficult because of the anisotropy in turbulence, leading to failures of the Boussinesq hypothesis in modeling the Reynolds stress and the conventional ε-equations in predicting the turbulence dissipation.[4] The anisotropy is caused by the strong swirl effect and the dominance of the turbulence fluctuations in the tangential and axial directions over that in the radial direction. The anisotropy in Reynolds stress can be accounted for by using a turbulence model, such as the Reynolds stress transport (RST) model, which individually calculates different components of the Reynolds stresses. Such models are readily available in commercial computational fluid dynamics (CFD) packages. To remedy the failure of conventional ε-equations, Malhotra et al.[5] attempted to improve the ε formulation by modifying its modeling constants. However, this issue is not addressed in commercial CFD packages.

In the area of numerical simulations of conical cyclones, researchers have been able to predict the velocity profiles using a modified κ–ε model.[5,6] These models required case-dependent empirical modifications and are not suitable for general engineering modeling purposes. Such empirical modifications are not necessary in an algebraic Reynolds stress model[7] or an RST model. An RST model, or its pressure–strain correlation in particular, can be either a linear model such as that proposed by Launder et al.[8] (LRR) or a quadratic model such as that proposed by Speziale et al.[9] (SSG). Representative studies using RST models are shown in Table 1.

From Table 1, one can conclude from Hoekstra et al.[10] that the LRR RST model can accurately model hydrocyclone flow up to a swirl number of 3.1. However, Cambon et al.[13] reported that in the presence of background rotation, the deviatoric terms in the rapid pressure–strain term in the LRR RST model disappear, which would make this model unsuitable for modeling swirling flows. This observation is in agreement with the study by Montavon et al.,[11] where the unsteady-SSG RST model was shown to be superior to the LRR RST model in predicting the velocity profiles. Although the failure of the LRR RST model can likely be attributed to a large swirl magnitude, this correlation cannot be definitely established

Table 1. A Summary of Validated Cyclone RANS Simulations

Primary Author	Sw*	Re**	Model Used	Data†	Comments‡‡
Hoekstra[10]	3.1	1.3×10^5	Steady-LRR	***TA***	Gas, 290 mm
Montavon[11]	Unknown	Unknown	Unsteady-SSG	***T***	Liquid, 36 mm
Harwood[12]	4.1	2.7×10^5	RST model§	***TA***	Gas, 205 mm

*Geometric swirl number.
**Reynolds number based on inlet velocity and the cyclone diameter.
†Validation through marginal tangential velocity (***T***) and axial velocity (***A***).
‡Fluid type and cyclone diameter.
§The pressure–strain correlation was not specified.

because the swirl number was not reported. Simulating the swirling flow generated by an axially rotating pipe wall with a one-dimensional and two-componential model, Pettersson et al.[14] showed that the SSG RST model was superior to a linear and a cubic model for flows with increasing system rotation. The flow in a hydrocyclone is at least two-dimensional and three-componential and it is not evident that the failure of the LRR RST model in Montavon et al.[11] can also be attributed to the increasing system rotation.

The objective of this study is to establish a general methodology for modeling swirling flows in hydrocyclones used for fiber fractionation. In such cases, the swirl number can be expected to be high and modification of the geometry of the hydrocyclone is of interest. Therefore, the attention is paid to applying the method on a nonconventional geometry at substantially higher swirl numbers than those already used in the industry. In particular, it is important to elucidate the applicability of the LRR and SSG RST models for flows with such high swirl numbers. The applicability of these models will be verified with the experimental results from Bergström.[15] In this experimental study, the tangential velocity profiles in a through-flow cylindrical hydrocyclone were obtained by extrapolating the pressure measurements from a pitometer.

To the best of the authors' knowledge, there have been no previous numerical studies of a through-flow cylindrical hydrocyclone. The combination of a novel geometry and a high swirl number will provide a general and rigorous examination of the performance of the two RST models. To objectively judge the performance of the RST models, care was taken to ensure that the only variable between the two simulations was the turbulence model and that all the other physical and numerical parameters in the simulations were kept identical as much as the solution convergence allowed.

This article is organized in the following manner. Details of the geometry and operating conditions modeled are outlined in the next section concerning the Problem Statement. Method of Solution describes the numerical model used. In Results and Discussion, the effect of nonuniform inlet velocity contours is shown before the simulated tangential velocity profile is validated against the experimental data. Then the axial velocity and radial velocity calculated are shown followed by discussions on the turbulence characteristics in the hydrocyclone. A final summary concludes this presentation.

Problem Statement

The hydrocyclone investigated herein is a through-flow cylindrical hydrocyclone whose detailed drawing is shown in Figure 2. Two connected volumes of the hydrocyclone are marked with different shades: the hydrocyclone, consisting of the inlets, the outlet, and the cylindrical body, is represented by the shadowed region and inlet chamber by the hatched region. The fluid enters the inlet chamber through one tangential pipe before it is injected into the hydrocyclone by three smaller tangential inlets. The swirl flow proceeds upward in the cylindrical main body until it exits as the reject or the accept flow. The reject flow exits through a tangential pipe and the accept flow through a vertical vortex finder. The vortex finder mouth in the experiment is located at a vertical height of 410 mm and its straight section extends to a vertical height of 800 mm. The

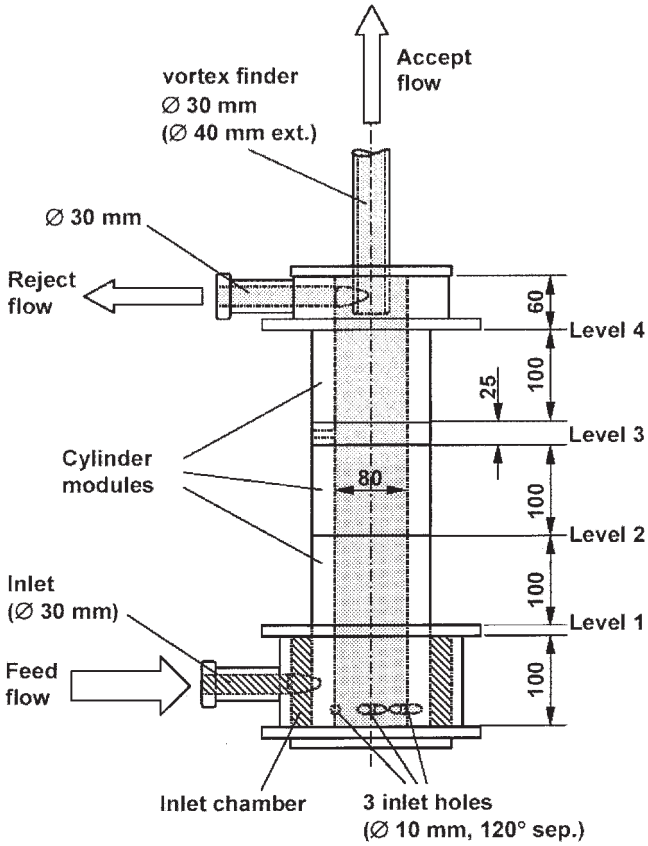

Figure 2. Geometry of the experimental hydrocyclone geometry.

straight section of the reject pipe has a length of 400 mm with its centerline at the vertical position of 457.5 mm.

The magnitude of the swirl created by the tangential inlets is quantified by the swirl number. The swirl number's integral definition relates the ratio between the axial fluxes of the angular and axial momentums and is written as

$$Sw_{\text{int}} = \frac{\int_0^{2\pi}\int_0^0 \rho U_z U_\theta r dr d\theta}{\int_0^{2\pi}\int_0^0 \rho U_z^2 r dr d\theta} \tag{1}$$

where U_z is the axial velocity, U_θ is the tangential velocity, and r_0 is the hydrocyclone radius. Because these velocities cannot be known a priori, a geometric swirl number based on the ratio of mass flows through the hydrocyclone and inlet cross-sectional areas can also be defined[10] and it is written as

$$Sw_{\text{geo}} = \frac{\pi d_{vf} D}{4A_{in}} \tag{2}$$

where A_{in} is the total area of the tangential inlets and d_{vf} and D are the diameters of the vortex finder and the hydrocyclone, respectively. The geometric swirl number of the cylindrical hydrocyclone is 8.1. It is much larger than values measured in other hydrocyclones, where swirl numbers < 4.1 are reported. The Reynolds number of the hydrocyclone is commonly defined with the tangential inlet velocity and the hydrocyclone diameter. The feed flow rate of the experiment was 2 L/s

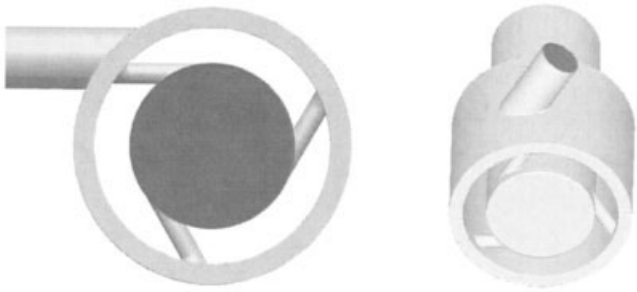

Figure 3. Geometry of the inlet chamber that was modeled separately to determine the effects of nonuniform inlet velocity profiles.

The top view on the left shows the single feed pipe entering the inlet chamber and the three small tangential inlets that connect the inlet chamber to the main hydrocyclone body. The figure on the right shows the vertical positions of the feed inlet and the three tangential inlets.

through the hydrocyclone, which corresponds to a Reynolds number of 6.8×10^5 in the present case. The present Reynolds number is also large compared to values reported in previous studies.

Method of Solution

The commercial CFD software package Fluent™ (version 6.1, Fluent, Inc., Lebanon, NH) was used in this study to compare the abilities of two different turbulence models in simulating highly swirling flow, with the aim of developing a general engineering methodology in modeling hydrocyclone flows having a range of swirl numbers. Two versions of the RST model will be tested. The same mesh will be used and all physical variables and numerical methods are kept constant unless a change was necessary to achieve solution convergence. Because the details of the turbulence models and the numerical methods used are well documented in the literature, this section will comment only on the issues relevant to the modeling of highly swirling hydrocyclone flows. The modeled geometries and their meshes will be discussed first, followed by a discussion on the turbulence models and the numerical methods.

The geometry of the hydrocyclone consists of two sections: the inlet chamber and the main hydrocyclone body. They occupy 13 and 87% of the total volume. The feed flow enters the inlet chamber by a single tangential pipe before the fluid is injected into the main body by three smaller inlets. The singular tangential feed pipe reduces the uniformities among the velocity contours of the three smaller inlets and the nonuniform contours can be determined only by modeling the entire inlet chamber. However, the flow in the inlet chamber is of no interest to the study unless the nonuniform inlet contours significantly affect the main hydrocyclone flow. For engineering purposes, it would also be desirable to replace a detailed simulation of the inlet chamber with a uniform velocity contour at the three tangential inlets. To investigate this assumption, the inlet chamber in Figure 2 was modeled separately. Details of the modeled inlet chamber geometry are shown in Figure 3.

The mesh generator used was Gambit 1.2 (Fluent Inc.). Most of the hydrocyclone was meshed using a "butterfly" scheme that divides the body into five sections consisting of hexahedral elements, as shown in Figure 4. This meshing scheme improves the results because the mesh elements are aligned with the flow direction and skewed cell elements at the center are avoided.[16] The tangential intersections between the pipes and the hydrocyclone body were meshed using tetrahedral elements that can be observed in the top right-hand corner in Figure 4. Adjacent faces between these regions were mapped to each other accordingly.

The flow in the simulated hydrocyclone is sensitive to the outlet boundary conditions used. The outflow boundary condition was used at both the reject and accept. It uses a zero diffusion flux to all the flow variables. It also assumes the flow

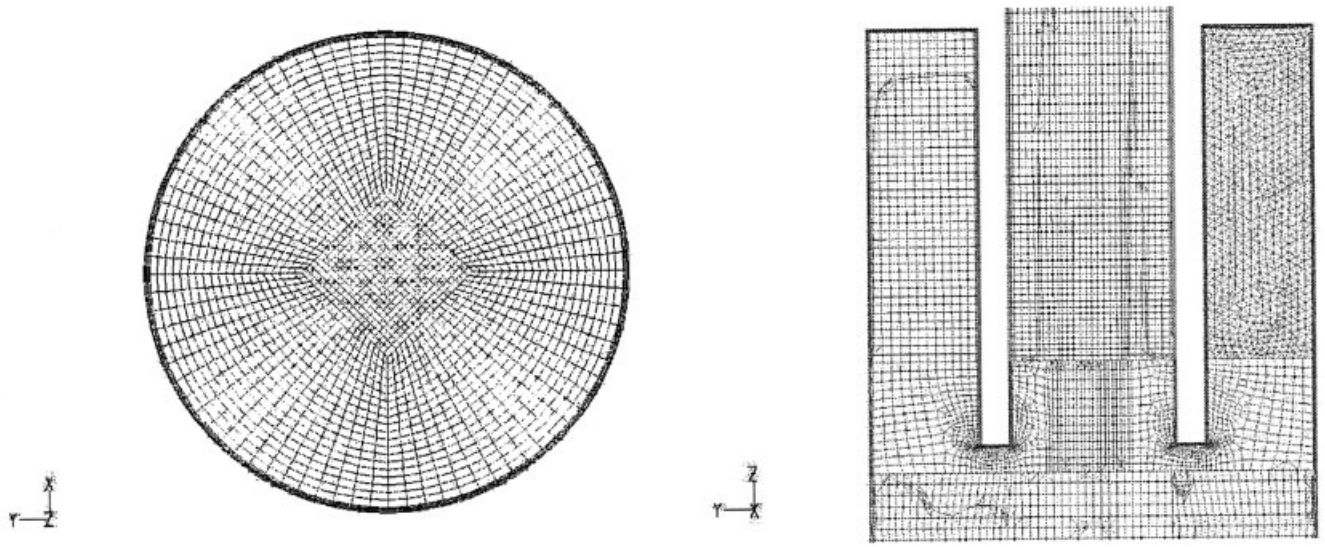

Figure 4. Details of the mesh created by Gambit 1.2.

The left figure shows the details of mesh at a cross section in the hydrocyclone body and the right figure shows details of the mesh near the vortex finder.

to be fully developed and the gradients of the variables to be zero in the cross-stream direction. Thus the lengths of the vortex finder and the tangential reject pipe were made much longer than those in the experiment to ensure that the above requirements of the outflow boundary condition were satisfied.

It is well known that the RST model, which individually calculates the transport equations for each Reynolds stress, is necessary to accurately model swirl flows in hydrocyclones. The two different RST models used were the LRR and the SSG RST models. The Reynolds stress transport equation can be expressed as

$$\frac{\partial}{\partial t}(\rho\overline{u_i u_j}) + \frac{\partial}{\partial x_k}(U_k\rho\overline{u_i u_j}) = P_{ij} + \phi_{ij} + D_{ij} - \varepsilon_{ij} \quad (3)$$

where P_{ij}, ϕ_{ij}, D_{ij}, and ε_{ij} are production, pressure–strain correlation, diffusion, and dissipation terms. Terms that require additional modeling are ϕ_{ij}, D_{ij}, and ε_{ij}. The turbulent term in D_{ij} is modeled with the formulation from Lien and Leschzier,[17] written as

$$D_{ij} = \frac{\partial}{\partial x_k}\left[\left(\mu + \frac{\mu_t}{\sigma_k}\right)\frac{\partial}{\partial x_k}(\overline{u_i' u_j'})\right] \quad (4)$$

The scalar dissipation rate ε-equation is defined similarly to the κ–ε model and the dissipation tensor ε_{ij} is modeled as

$$\varepsilon_{ij} = \frac{2}{3}\delta_{ij}\rho\varepsilon \quad (5)$$

The LRR and SSG RST models used in this study differ in their formulations of the pressure–strain correlation, which predicts how the Reynolds stress components are redistributed in the flow. The pressure–strain correlation is a sum of a return to isotropy term (ϕ_{ij}^1) and a rapid pressure–strainterm(ϕ_{ij}^2) . ϕ_{ij}^1 accounts for the effects of pressure on the Reynolds stress and it will always act to increase the isotropy in the Reynolds stress distribution, as its name suggests. ϕ_{ij}^2 is called the rapid pressure–strain term because it includes the effect of the mean rate of strain, which has a more immediate impact on the Reynolds stresses. This term is particularly important in the modeling of swirling flows. The LRR RST model includes linear terms of the turbulence anisotropy and is calibrated against homogeneous and inhomogeneous shear flows.[8] The wall reflection term was not used because its inclusion did not improve the agreement between the LRR RST results and the experiments. The SSG RST model includes quadratic terms in the turbulence anisotropy. Its validation included rotation shear flows, in addition to other homogeneous turbulent flows.[9] Because the difference between the pressure–strain correlations of the two models is compared in this study, the details of these terms are presented below.

Using the notation in Pope[18] the pressure–strain correction terms are defined. The return to isotropy term ϕ_{ij}^1 in the LRR RST model is

$$\frac{\phi_{ij,LRR}^1}{\rho\varepsilon} = -2C_R b_{ij} \quad (6)$$

where C_R is 1.8. b_{ij}, the normalized Reynolds-stress anisotropy, is defined as

$$b_{ij} = \frac{\overline{u_i' u_j'}}{2k} - \frac{1}{3}\delta_{ij} \quad (7)$$

In the SSG RST model, $\phi_{ij}^1$is defined as

$$\frac{\phi_{ij,SSG}^1}{\rho\varepsilon} = -\left(C_1 + C_1^*\frac{P}{\varepsilon}\right)b_{ij} \quad (8)$$

In addition to C_1 and C_1^*, whose values are 3.4 and 1.8, respectively, the model coefficient is a function of the ratio between the trace of the rate of production of the Reynolds stress P and the dissipation ε.

The more significant difference lies in the rapid pressure–strain term, ϕ_{ij}^2. Excluding the wall reflection term, ϕ_{ij}^2 in the LRR RST model is defined as

$$\frac{\phi_{ik,LRR}^2}{\rho\varepsilon} = \frac{4}{3}C_2\hat{S}_{ij} + 2C_2\left(\hat{S}_{ik}b_{kj} + b_{ik}\hat{S}_{kj} - \frac{2}{3}\hat{S}_{kl}b_{lk}\delta_{ij}\right) + 2C_2(\hat{\Omega}_{ik}b_{kj} + b_{ik}\hat{\Omega}_{kj}) \quad (9)$$

where the constant C_2 has a value of 0.6. $\hat{S}_{ij}$ is the rate of strain tensor and $\hat{\Omega}_{ij}$ is the rate of rotation tensor, both normalized by $2k$. ϕ_{ij}^2 in the SSG RST model is defined as

$$\frac{\phi_{ij,SSG}^2}{\rho\varepsilon} = C_2\left(b_{ij}^2 - \frac{1}{3}b_{kk}^2\varepsilon_{ij}\right) + (C_3 - C_3^*\sqrt{b_{ij}b_{ij}})\hat{S}_{ij} + C_4\left(\hat{S}_{ik}b_{kj} + b_{ik}\hat{S}_{kj} - \frac{2}{3}\hat{S}_{kl}b_{lk}\delta_{ij}\right) + C_5(\hat{\Omega}_{ik}b_{kj} + b_{ik}\hat{\Omega}_{kj}) \quad (10)$$

where the constants are C_2=.2, C_3=.8, C_3^*=.8, C_4=.25, and C_5=.4. The inclusion of the term following C_2 gives the SSG RST its nonlinear return to isotropy behavior.

A Reynolds number based on the mean axial velocity and hydrocyclone diameter gives a clearer indication of the turbulence level in the main hydrocyclone body, and it is 5.0×10^5. In contrast, the Reynolds number based on the inlet velocity and inlet diameter is 8748. Despite the low magnitude of the Reynolds number at the inlet, the inlet chamber contributes to a high level of inlet turbulence level. Therefore, the use of the RST models over the entire flow domain is appropriate.

Near the wall, the flow in the boundary layer is modeled using the wall functions. The conventional standard wall function assumes that the turbulence energy production and dissipation rate are equal near the wall, which can be inaccurate when there exists a large pressure gradient parallel to the wall in the direction of the mean flow, as in the case of confined swirling flows. A nonequilibrium wall function proposed by Kim and Choudhury[19] attempts to correct this assumption by adjusting the log-law of the near-wall velocity to the pressure gradient and by calculating the turbulence energy budget in two separate sublayers. Both the standard and the nonequilibrium wall functions were tested in this study.

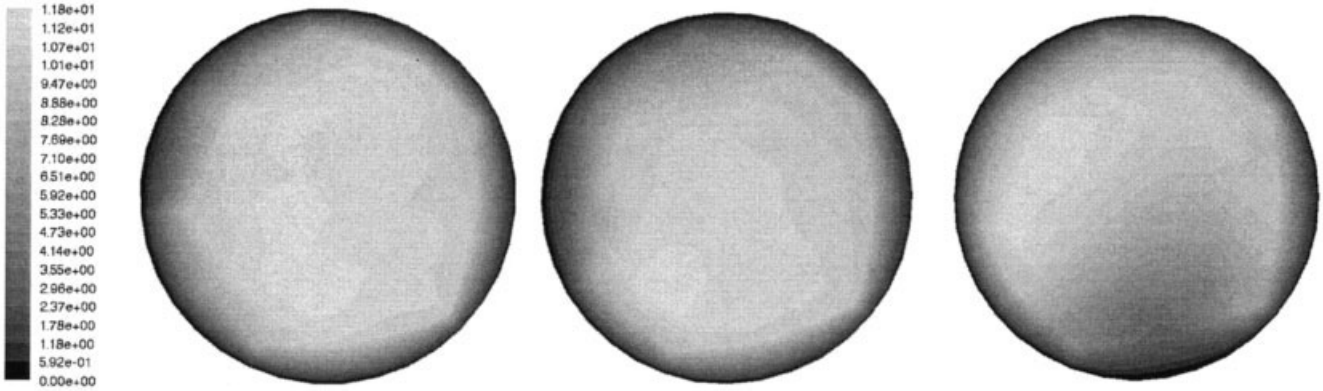

Figure 5. Nonuniform velocity contours created by the inlet chamber at the three small inlets entering the main body of the hydrocyclone, as viewed from the inlet chamber tangentially into the hydrocyclone main body.

The velocity has a unit of m/s.

The Navier–Stokes equations with the above-mentioned turbulence closure models were discretized and solved. Because variable values are stored at the cell volume centers, the cell face values must be interpolated. To avoid numerical diffusion, the QUICK™ scheme was used in discretization of the momentum equations. The second-order scheme was used for the ε and Reynolds stress equations to avoid the nonphysical behavior described in Tsao and Lin.[20] PRESTO™ was used as the pressure discretization scheme and SimpleC™ was used for the pressure–velocity coupling.

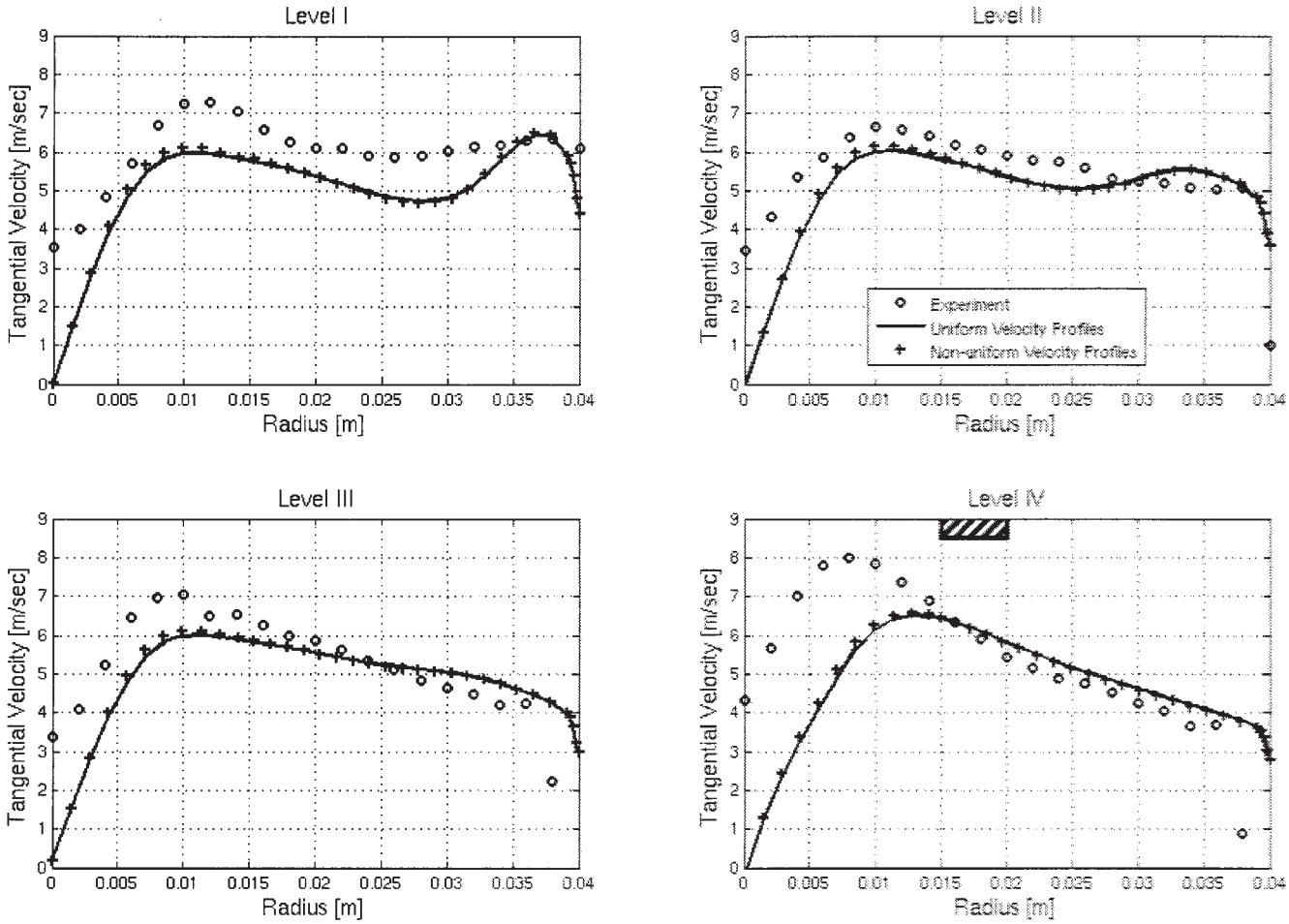

Figure 6. Comparison of the effects of the nonuniform inlet velocity contours on the tangential velocity profiles at the four vertical levels in the hydrocyclone in Figure 2.

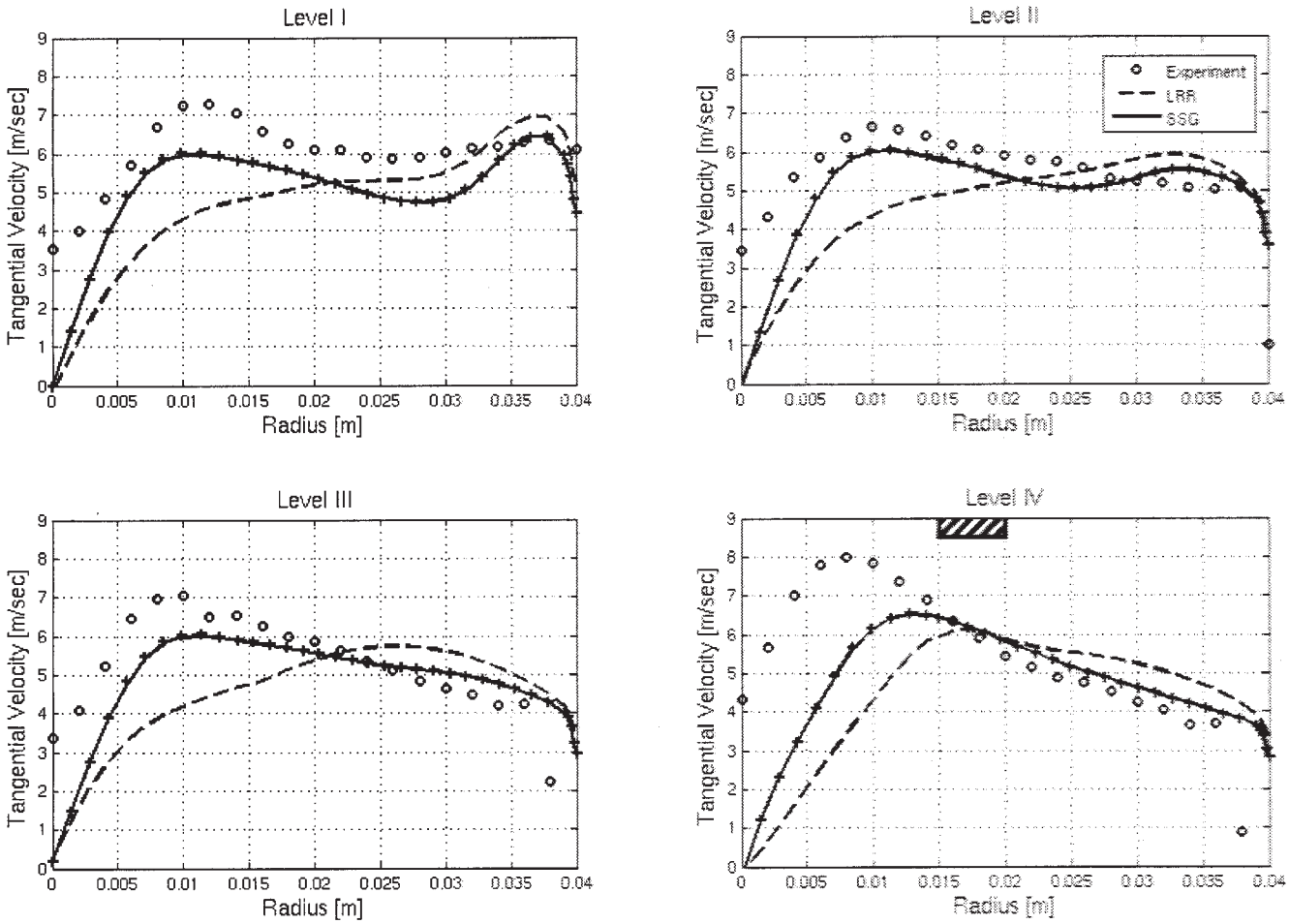

Figure 7. Comparison of the tangential velocity between the experiment and the LRR and SSG RST simulations at the four different vertical levels shown in Figure 2.

The hatched box shows the radial position of the vortex finder just above Level IV. The SSG RST velocity profiles from the 2.8 million element case is shown with the crosses.

The inlet flow rate was defined as uniform velocity contours. The amount of flows through the reject and accept were equal in the experiment. In the simulation, this was modeled by defining the flow rate weighting to be 50% at both outlets. The boundary condition at the outlets was defined as outflow. The experiment was operated with an air core, which was not included in the simulations.

The above-mentioned numerical method has been also validated by the authors using experimental data of pipe swirling flows created by tangential inlets.[21] Details about this validation study can be found in Ko.[22]

Results and Discussion

In this section, the effect of nonuniform inlet flows will be shown first and then the flows in the hydrocyclone simulated using the LRR and the SSG RST models will then be presented.

The flows that enter the hydrocyclone through the three tangential inlets have an average velocity of 8.74 m/s, although the velocity contours at these tangential inlets do not need to be identical and uniform because of the inlet chamber. The inlet chamber, with its single tangential feed pipe, three small tangential inlets, and a portion of the main hydrocyclone body, was modeled to determine the nonuniform velocity contours at the three tangential inlets. These contours are shown in Figure 5. The variations among and within the inlets can be clearly observed. The average velocity magnitudes at the three inlets are 8.21, 8.72, and 9.29 m/s, with a total average of 8.74 m/s. To determine the difference between uniform and nonuniform inlet velocity definitions, the contours shown in Figure 5 were then used as the inlet velocity definition in a simulation of the flow in the main body of the hydrocyclone.

The comparison between the experimental measurements and simulation results obtained from uniform and nonuniform inlet velocity contours is shown in Figure 6. The tangential velocities calculated from nonuniform velocity contours show no differences compared to the uniform velocity contours. Thus, the uniform inlet velocity contours were sufficient approximations and were used for all the simulations in this study. The differences in the axial velocity profiles were also negligible.

The steady and unsteady solvers were tested. The LRR RST model was solved using both steady and unsteady solvers and there was no difference in the tangential velocity solutions.

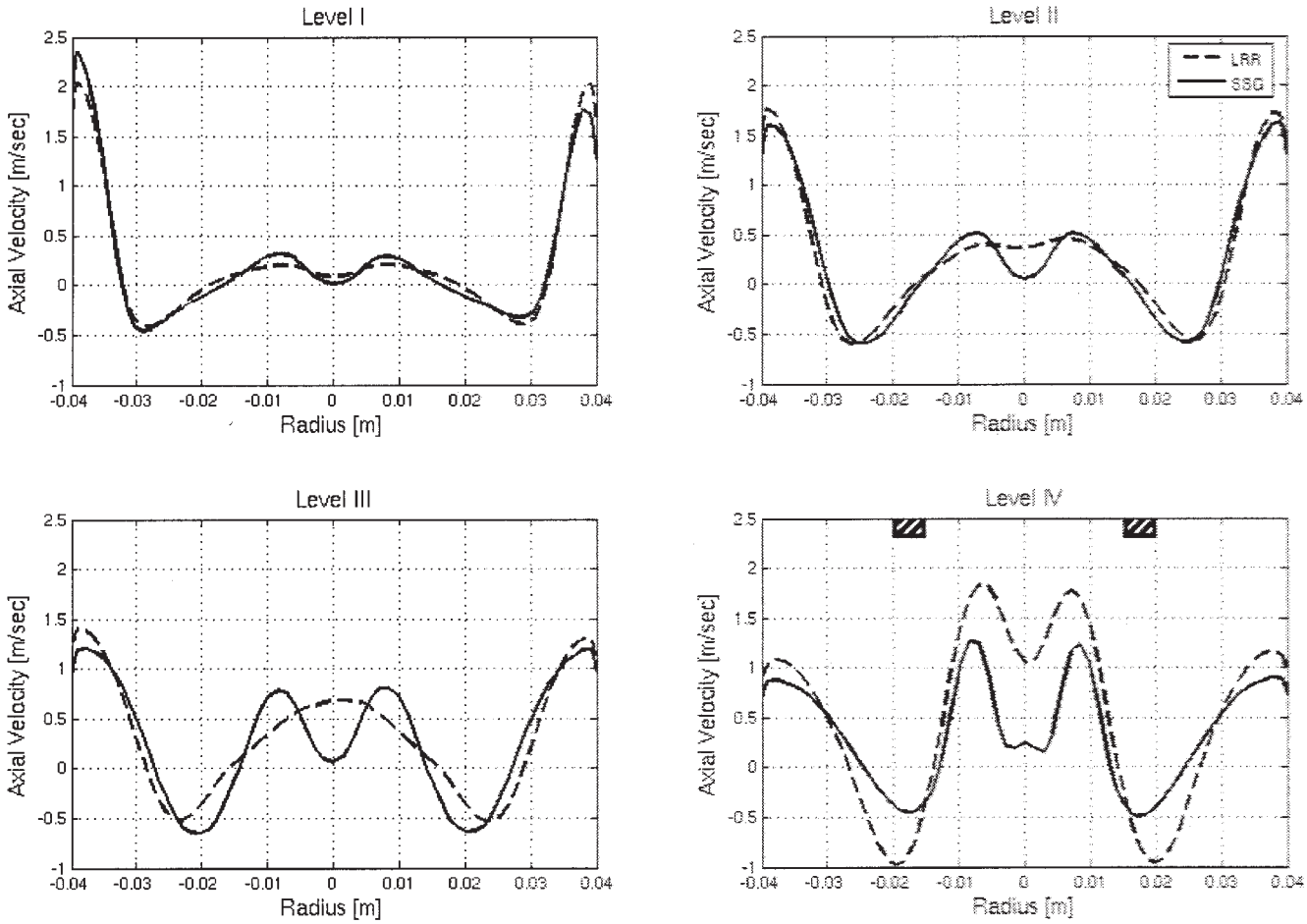

Figure 8. Comparison of the axial velocity between the LRR and SSG RST simulations at the four different vertical levels shown in Figure 2.

The hatched box shows the radial position of the vortex finder just above Level IV.

However, the SSG RST model diverged in the steady solver and converged only in the unsteady solver. The average fluid residence time in the hydrocyclone is 1.34 s and the time step in the unsteady solver was set to 0.01 s. The velocity profiles from both solutions shown below represent time-averaged values taken over 1.50 s. In addition, the definition of the wall functions was found to be crucial for the solution convergence. The LRR RST model converged only with the nonequilibrium wall function and the SSG RST model converged only with the standard wall function. Besides the turbulence models, the wall function is the only necessary difference between the two sets of results presented.

After the modeling parameters were established, mesh dependency studies were performed. Refinement up to 2.8 million mesh elements was done, although tangential velocity profiles at the four levels from different cases showed only slight changes above 0.85 million mesh elements for both the LRR and the SSG RST models, as shown in Figure 7. The 2.8-million element mesh has a distribution of approximately 50, 160, and 300 elements, in the radial, tangential, and axial directions, respectively; the 0.85-million element mesh has a distribution of approximately 34, 80, and 220 elements. The simulations discussed in the remaining part of this article are calculated with the 0.85-million element mesh.

In the experiment by Bergström,[15] the tangential velocities were measured from the hydrocyclone wall to the geometric center at Levels I to IV, as shown in Figure 2. The tangential velocity profiles are shown in Figure 7. There are two dominant features in the experimental measurements. First, a Rankine's combined vortex is observed at all four levels. As described previously, the Rankine vortex is commonly observed in hydrocyclone flows. Second, the peak value of the tangential velocity profile at Level IV is elevated. The cross-sectional area of the vortex finder corresponds to 14% of the total hydrocyclone cross-sectional area, but 50% of the outflow exits through the vortex finder. As the outflow is forced into this small area, the conservation of the angular momentum leads to an increase in the tangential velocity below the vortex finder. The simulated tangential velocity profiles were examined at other angular positions and were found to be the same. Thus the nonaxisymmetric effect is not the cause of the phenomena described below.

The two RST models were able to predict the two above-mentioned features to varying degrees. The LRR results do not have a Rankine vortex pattern at the lower three levels but show an increased tangential velocity at Level IV. The absence of the Rankine vortex in the LRR solution shows that the model is unable to capture all features of highly swirling flows. This

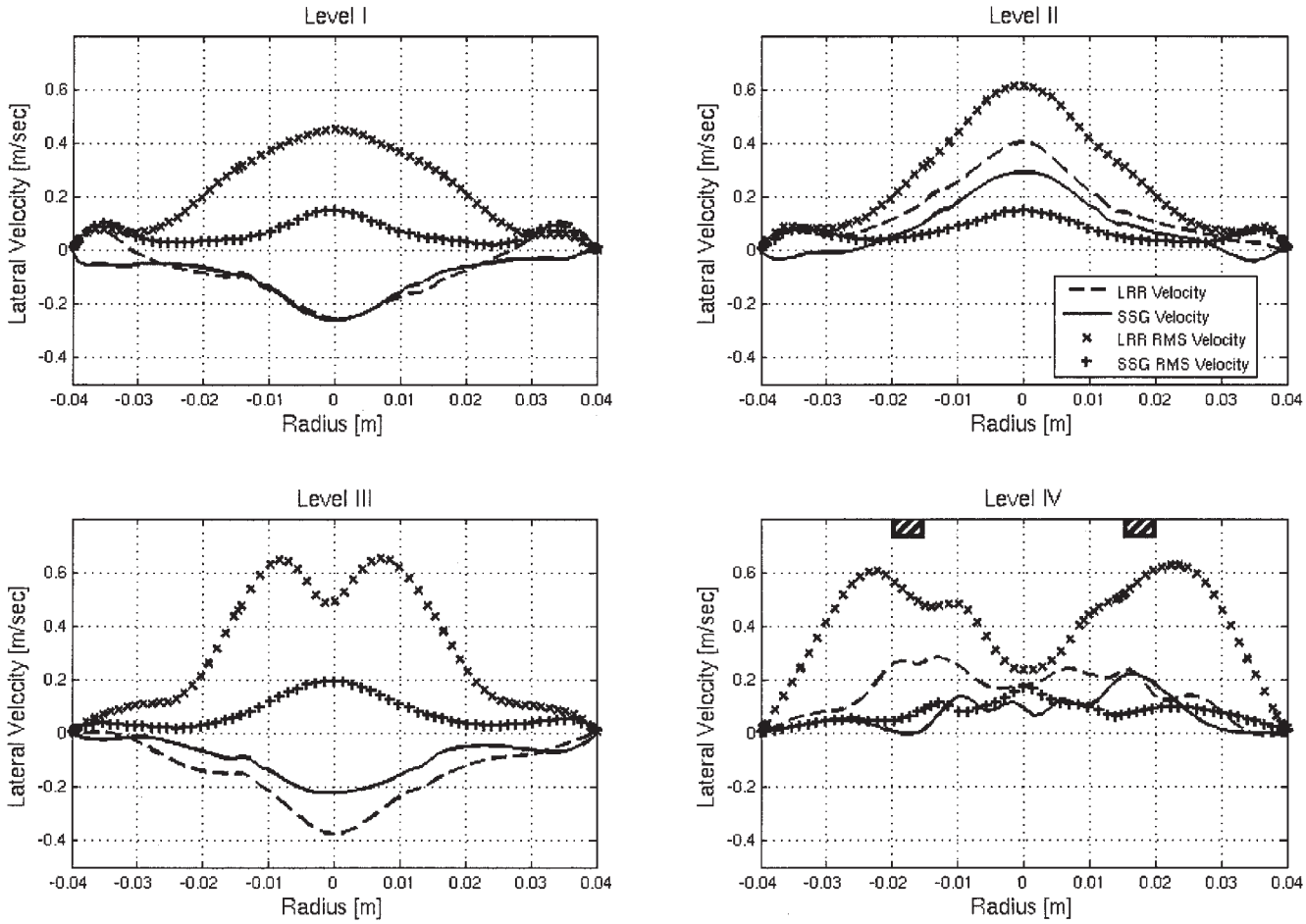

Figure 9. Comparison of the average lateral velocity and its rms values taken over 1.50 s from the LRR and SSG RST simulations.

The hatched boxes show the radial positions of the vortex finder just above Level IV.

observation confirms the shortcomings of the linear model of the pressure–strain correlation in LRR (see, for example, Montavon et al.[11] and Pettersson et al.[14]). In contrast, the SSG results were more successful in predicting both features. The Rankine vortex could be observed at all levels, which shows that SSG is more suitable in modeling highly swirling flows. Overall, both the velocity magnitudes and the increased tangential velocity on Level IV predicted by the SSG RST model are in good agreement with experimental results. More important, in combination with the results from Hoekstra et al.,[10] one can establish that the limit of LRR RST model lies between swirl numbers of 3.1 and 8.1. The threshold range of the LRR RST model's applicability could be narrowed by further studies.

Close examination of the experimental data shows nonzero tangential velocities at the geometric center, which are likely to be caused by the interference of the air–water interface with the pitometer. In the experiment the air core has a radius up to 3.5 mm and precesses in an oscillatory pattern about the geometric center.[15] Consequently, it would have immediate effects on the fidelity of, at least, the three innermost measurement points. Because the simulations included only the water phase and air was omitted, the tangential and radial velocities at the geometric center had to be zero. Therefore, the comparison of the velocity profiles near the geometric center must be considered with caution.

The numerical axial velocity profiles are shown in Figure 8 and the results will be discussed only with respect to the two RST models, given that no experimental data are available. The simulated axial velocity profiles from both models show a coannular flow reversal region. Previous studies showed that the extent and the magnitude of the flow reversal in a pipe swirl flow increase with increasing swirl number.[21] At the high swirling number of the current hydrocyclone, the axial flow reversal is extensive and its magnitude large. Because the hydrocyclone's fractionation ability comes from the large centrifugal acceleration imparted on the flow constituents, it would be desirable to have a stable plug flow even when the swirl number becomes large. Therefore, fractionation hydrocyclones with long cylindrical sections must be operated with care to avoid increased vertical mixing that could be introduced by the axial flow reversal.

Although the inlets are defined with steady uniform velocity profiles, an unsteady solver was used. As explained earlier, the unsteady solver is needed to obtain a converged solution for the quadratic SSG RST model. Physically, the unsteady solver is

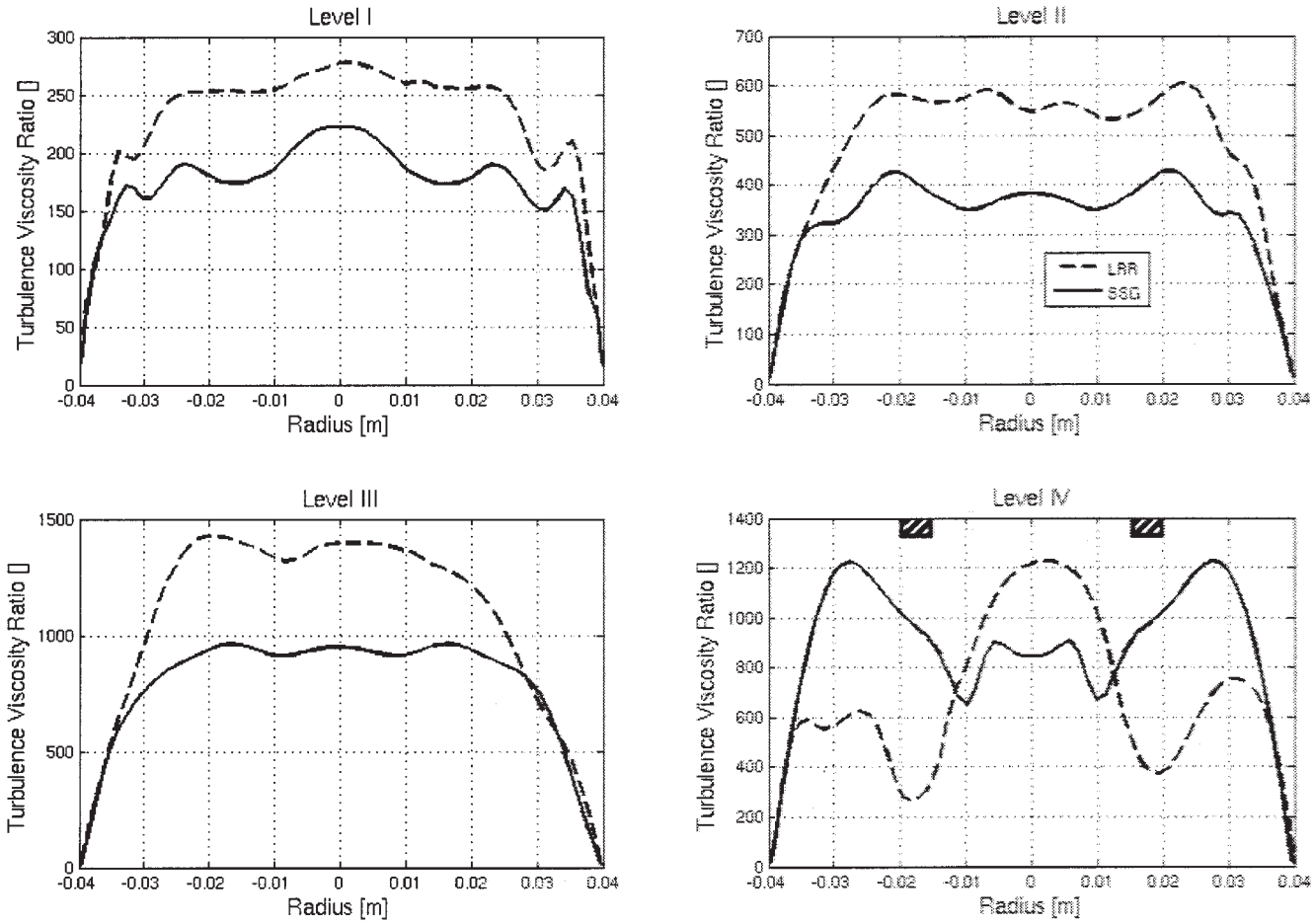

Figure 10. Comparison of the instantaneous turbulent viscosity ratio from the LRR and SSG RST simulations at 1.50 s at all four levels.

needed to resolve the large-scale precessing motion of the vortex core. In a swirling flow, the large centrifugal force creates a low-pressure column near the geometric center of axis. This vortex core precesses at a high frequency and causes large fluctuations in the radial velocities. This oscillatory motion exists independently of the steady boundary condition and can be accurately resolved using only the unsteady solver.

In previous numerical studies, there has not been much information on the radial velocity components. They are often small compared to the tangential or the axial components and are difficult to measure. In addition, the oscillation from the PVC makes the variation in the radial velocity large and even more difficult to measure. When plotting the radial velocity over the hydrocyclone diameter, the velocity profiles become discontinuous at the geometric center. To avoid this discontinuity and to better demonstrate the PVC structure, the negative values of the radial velocity are used in the area where the radius is negative. This resultant velocity profile shows the lateral PVC motion and will be called the *lateral velocity*. Figure 9 shows the simulated lateral velocity and their root-mean-square (RMS) values. The maximum lateral velocities are roughly one-tenth and one-thirtieth of the maximum axial and tangential velocities on their corresponding levels. The lateral velocities have negative values on Levels I and III and positive values at Level II, which suggests that the PVC has a preferred helical position in the hydrocyclone that is not axisymmetric. In a previous study of a reverse-flow cylindrical hydrocyclone, a helical shape was also observed in the position of the PVC.[23] The RMS lateral velocity values shown in Figure 9 are taken over a simulation time of 1.50 s. In the LRR solution, the lateral RMS values are clearly larger than the magnitude of the lateral velocity at all the levels. In contrast, the SSG RSM values are approximately as large as the lateral velocity profiles.

Previous studies showed that a decrease in the turbulent kinetic energy occurred at large swirl numbers in cases involving swirling flow generating by a rotating pipe wall.[24] Such relaminarization in swirl flow would make the application of turbulence models invalid. To determine the degree of relaminarization, the turbulence intensity was monitored on Levels I to IV. The turbulence intensity is defined as

$$I = \frac{\sqrt{(3/2)k}}{V_{ref}} \tag{11}$$

where V_{ref} is the reference velocity, which is defined as the main axial velocity, 0.396 m/s; and k is the turbulent kinetic energy, determined by taking the trace of the Reynolds stresses. If relaminarization does occur as a result of the high swirl, the

turbulence intensity should decrease as the flow approaches the vortex finder. However, the averaged turbulence intensities on Levels I to IV are 28.55, 43.07, 61.09, and 68.58. Instead of relaminarizing, the turbulence intensity increased as the flow approaches the vortex finder.

The magnitude of turbulence can also be observed by the turbulent viscosity ratio, which is the ratio between the turbulent and fluid viscosities, determined with the turbulent kinetic energy also calculated from the trace of the Reynolds stresses. Figure 10 shows the instantaneous ratio at 1.50 s at all four levels. It shows that the turbulent viscosity ratio increases as the flow approaches the vortex finder and no relaminarization occurs. The relaminarization of the fluid is prevented likely as a result of the large magnitude of axial velocity gradients.

Conclusion

The flow in a cylindrical through-flow hydrocyclone was simulated using Fluent™ with both a linear (LRR) and a quadratic (SSG) model for the pressure–strain correlation term in the Reynolds stress transport (RST) model with both steady and unsteady solvers. The methodology used does not depend on any case-specific adjustments and therefore can be applied to any cyclone geometry under a wide rage of operating conditions. A coarse and a fine mesh were both tested to ensure mesh independence and no difference was observed in the results. All physical and numerical parameters required to achieve converged solutions were determined and presented. Despite the large swirl number and the nonconventional geometry of the hydrocyclone, the results obtained using the SSG RST model were in good agreement with experimental tangential velocity data, whereas shortcomings in the LRR RST model were illustrated. Important features of the swirling flow in hydrocyclones, such as the Rankine vortex and an elevated tangential velocity near the vortex finder, were correctly predicted by the SSG RST model. Both models predicted a large amount of flow reversal in the axial direction of the hydrocyclone. Such a flow reversal can be undesirable in a fractionation process. Hydrocyclone design and operation thus need to consider the relative effects on fiber stratification from the separation by the centrifugal force and from the enhanced mixing by the axial flow reversal. The use of the unsteady solver explores a physical feature of strongly swirling flow, that is, the existence of large-scale fluctuations arising from the vortex core, which exist despite the steady boundary conditions. In combination with the SSG RST model, a methodology in simulating strongly swirling flows in a general geometry has been developed and validated.

Acknowledgments

The financial supports from ECOTARGET, the Swedish Foundation for Strategic Research Multiphase Flow Programme and STFI-Packforsk's partner companies participating in the research cluster "Advanced Fibre Management in Stock Preparation" are gratefully acknowledged.

Literature Cited

1. Demuner BJ. Opportunities for market pulp differentiation via fractionation. Proceedings of the 5th International Paper and Board Industry Conference, Scientific and Technical Advances in Refining, PIRA International, Vienna, Austria; 1999.
2. Kure K-A, Dahlqvist G, Ekstrom J, Torbjörn H. Hydrocyclone separation, and reject refining, of thick-walled mechanical pulp fibres. *Nordic Pulp Paper Res J.* 1999;14:100-104.
3. Paavilainen L. The possibility of fractionating softwood sulfate pulp according to cell wall thickness. *Appita.*1992;45:319-6.
4. Cambon C, Mansour NN, Godeferd FS. Energy transfer in rotating turbulence. *J Fluid Mech.*1997;337:303-2.
5. Malhotra A, Branion RMR, Hauptmann EG. Modelling the flow in a hydrocyclone. *Can J Chem Eng.* 1994;72:953-960.
6. He P, Salcudean M, Branion R, Gartshore IS. Mathematical modelling of hydrocyclones. Proceedings of the 1997 ASME Fluid Engineering Division Summer Meeting (FEDSM); 1997.
7. Boysan F, Ayers WH, Swithenbank J. A fundamental mathematical modelling approach to cyclone design. *Trans IChemE.* 1982;60:222-230.
8. Launder BE, Reece GJ, Rodi W. Progress in the development of a Reynolds-stress turbulence closure. *J Fluid Mech.* 1975;68:537-566.
9. Speziale CG, Sarkar S, Gatski TB. Modelling the pressure–strain correlation of turbulence: An invariant dynamical systems approach. *J Fluid Mech.*1991;277:245-2.
10. Hoekstra AJ, Derksen JJ, Van den Akker HEA. An experimental and numerical study of turbulent swirling flow in gas cyclones. *Chem Eng Sci.* 1999;54:2055-2065.
11. Montavon CA, Grotjans H, Hamill IS, Phillips HW, Jones IP. Mathematical modelling and experimental validation of flow in a cyclone. Proceedings of the 5th International Conference on Cyclone Technologies, Vortex Separation, York, UK; 2000:175-186.
12. Harwood R, Slack M. CFD analysis of a cyclone. *QNET Network Newsletter.*2002;1:25-.
13. Cambon C, Jacquin L, Lubrano JL. Toward a new Reynolds stress model for rotating turbulent flows. *Phys Fluids A.* 1992;4:812-824.
14. Pettersson BA, Andersson HI, Brunvoll AS. Modeling near-wall effects in axially rotating pipe flow by elliptic relaxation. *AIAA J.* 1998;36:1164-1170.
15. Bergström J. *Fiber Suspension Velocity Measurements in a Cylindrical Through-Flow Hydrocyclone*. Licentiate Thesis. Stockholm, Sweden: Royal Institute of Technology; 04.
16. Slack MD, Del Porte S, Engelman MS. Designing automated computational fluid dynamics modelling tools for hydrocyclone design. *Miner Eng.*2004;17:543-7.
17. Lien FS, Leschziner MA. Assessment of turbulent transport models including non-linear RNG eddy-viscosity formulation and second-moment closure. *Comput Fluids.* 1994;23:983-1004.
18. Pope SB. *Turbulent Flow*. Cambridge, UK: Cambridge Univ. Press; 2000.
19. Kim S-E, Choudhury D. A near wall treatment using wall functions sensitized to pressure gradient. Proceedings of theASME JSME Fluids Engineering and Laser Anemometry Conference and Exhibition;1995; 217:273-280.
20. Tsao JM, Lin CA. Reynolds stress modelling of jet and swirl interaction inside a gas turbine combuster. *Int J Numer Methods Fluids.* 1999;29:451-464.
21. Chang F, Dhir VK. Turbulent flow field in tangentially injected swirl flows in tubes. *Int J Heat Fluid Flow.* 1994;15:346-356.
22. Ko, J. *Numerical Modelling of Highly Swirling Flows in a Cylindrical Through-Flow Hydrocyclone*. Licentiate Thesis. Stockholm, Sweden: Royal Institute of Technology; 2005.
23. Derksen JJ. Separation performance predictions of a Stairmand high-efficiency cyclone. *AIChE J.* 2003;49:1359-1371.
24. Jakirlic S, Hanjalic K, Tropea C. Modelling rotating and swirling turbulent flows: A perpetual challenge. *AIAA J.* 2002;40:1984-1996.

Manuscript received Mar. 29, 2005, and revision received May 24, 2006.